



3D-printed microfluidic manipulation device integrated with magnetic array

Jie Wu¹ · Yiwen Cui¹ · Shouhu Xuan¹ · Xinglong Gong¹

Received: 17 July 2018 / Accepted: 25 August 2018 / Published online: 29 August 2018
© Springer-Verlag GmbH Germany, part of Springer Nature 2018

Abstract

This paper reported a transparent, high-precision 3D-printed microfluidic device integrated with magnet array for magnetic manipulation. A reserved groove in the device can well constrain the Halbach array or conventional alternating array. Numerical simulations and experimental data indicate that the magnetic flux density ranges from 30 to 400 mT and its gradient is about 0.2–0.4 T/m in the manipulation channel. The magnetic field parameters of Halbach array in the same location are better than the other array. Diamagnetic polystyrene beads experience a repulsive force and move away from the magnetic field source under the effect of negative magnetophoresis. It is undeniable that as the flow rate increases, the ability of Halbach array to screen particle sizes decreases. Even so, it has a good particle size discrimination at a volumetric flow rate of 1.08 mL/h, which is much larger than that of a conventional PDMS device with a single magnet. The observed particle trajectories also confirm these statements. The deflection angle is related to the magnetic field, flow rate, and particle size. This 3D-printed device integrated with Halbach array offers excellent magnetic manipulation performance.

Keywords 3D-printed device · Magnetic manipulation · Halbach array · Alternating array · Numerical simulations

1 Introduction

Microfluidic particles manipulation has a great importance in the biological and chemical applications in diagnostics (Merola et al. 2015; Yan et al. 2017), environmental monitoring (Cheng et al. 2016), and therapeutics (Gholizadeh et al. 2017; Kopp and Arosio 2018). Due to characteristics of simplicity, no heat generation, and non-invasive, the utilization of magnetic force for microfluidic applications has attracted intense interest from the research community. Magnetic manipulation has been used in a variety of applications such as pumping, separation, sorting, mixing, and magnetic wetting (Cao et al. 2017; Wyatt Shields et al. 2015; Yan et al. 2016). Typically, a single magnet was embedded in the device to generate magnetic field (Zhang et al. 2016; Zhou et al. 2016; Zhou and Xuan 2016). However, the magnetic field generated decreases sharply with increasing distance,

which affects the efficiency and convenience of magnetic manipulation (Khashan et al. 2018; Zhou et al. 2016; Zhu et al. 2011; Zhou and Xuan 2016). In 1980, Klaus Halbach proposed that assembling multipole permanent magnets with different polarization angles would increase the magnetic field on one side of the array while eliminating the magnetic field on the other side (Halbach 1980). However, the application of microfluidic magnetic manipulation has been limited by the large mutual repulsion between magnets and the Halbach array was not widely used. The previous researches on Halbach array have mostly concentrated on numerical simulations (Kang et al. 2016; Qiu et al. 2015; Salauddin et al. 2016) or using complex set screws (Zhou et al. 2017).

In addition, the fabrication of microfluidic manipulation chips mainly relies on soft lithography technology (Xia and Whitesides 1998) with elastic materials (polydimethylsiloxane, PDMS). The low elastic modulus of PDMS is easily deformed by large force (Gervais et al. 2006; Johnston et al. 2014). This makes the PDMS chips unable to restrain the above-mentioned magnet array. On the other hand, it is worth noting that 3D printing or additive manufacturing has been used to fabricate microfluidic devices based on a layer-by-layer addition process (Au et al. 2016; Gross et al. 2014; Yazdi et al. 2016). Many different techniques have

✉ Xinglong Gong
gongxl@ustc.edu.cn

¹ CAS Key Laboratory of Mechanical Behavior and Design of Materials, Department of Modern Mechanics, University of Science and Technological of China, Hefei 230027, People's Republic of China

been used for 3D printing microfluidics to produce complex and multi-level geometry, like stereolithography (SLA) (Lee et al. 2014), fused deposition method (FDM) (Chudobova et al. 2015), inkjet (Walczak and Adamski 2015), and selective laser sintering (Minocchieri et al. 2008). Some of the techniques were low in precision (Waheed et al. 2016). Some of them needed multi-steps to make 3D printing microfluidic devices (Ibi et al. 2018). In summary, this uncompetitive resolution, high cost, low transparency of the material (difficult to observe the internal situation of the channel), and difficulty in removing residual photosensitive resin from the sample have hampered the further application of 3D printing in microfluidics (Au et al. 2016; Ho et al. 2015). However, unlike to the PDMS chips, the larger elastic modulus of the 3D printed device makes it possible to integrate magnet array.

In this work, we have reserved a groove in the 3D-printed device to provide sufficient strength to constrain magnet array. Considering the fact that magnetic manipulation usually faces diamagnetic living cells, we described its handling abilities by analyzing the trajectories of micro-meter size diamagnetic polystyrene beads in ferrofluids. First, we showed the magnetic field and magnetic field gradient of the Halbach array and conventional alternating array at long distance, and then confirmed that the Halbach array outperformed the other array in both theoretical and experimental analyses. The negative magnetophoresis acted on particles is proportional to magnetic flux density and its gradient. Then, the numerical simulation results indicate that two particles sizes (5 μm PS beads, 12 μm PS beads) can be well distinguished in the channel width direction at a volumetric flow rate of 1.08 mL/h. This flow rate is tens to hundreds of times larger than that in the traditional PDMS chip with a single magnet (Kim and Park 2005; Zhou et al. 2016; Zhou and Xuan 2016). The observation of particle trajectories by a fluorescence microscopy verifies the conclusions of the

numerical simulations. The deflection angle of particle trajectory under Halbach array is greater than that of alternating array and decreases as the volumetric flow rate increases. The difference in deflection angles accounts for the particle sizes dependence in magnetic manipulation. Moreover, the 3D-printed material in this work is transparent, the processing precision is high, and the residual resin inside the sample is easy to be removed. These results indicate that the 3D-printed device integrated with Halbach array has excellent magnetic manipulation capabilities, and it will have a wide range of applications in particle sorting, separation, and mixing.

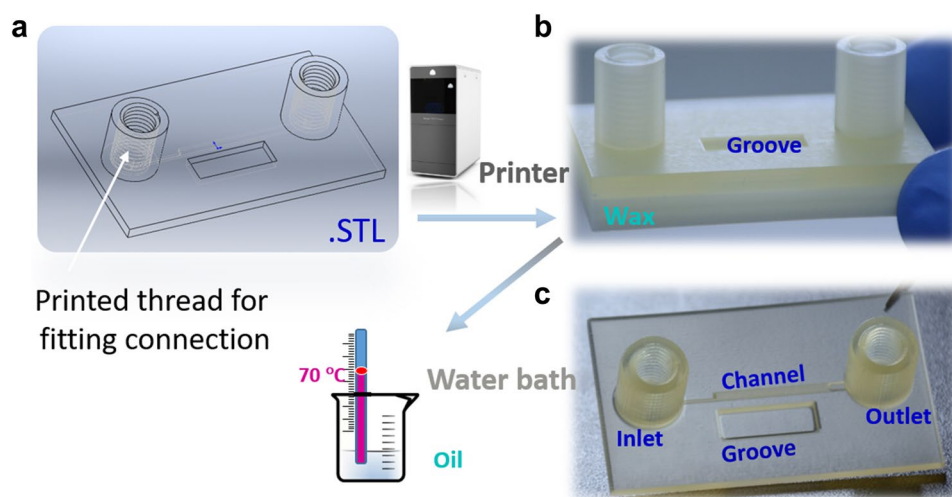
2 Materials and methods

2.1 Device fabrication

The devices were designed using SolidWorks 2013 (Dassault Systemes S.A, Inc., USA) to get solid part (.SLDPART) files. It is worth noting that SolidWorks generates virtual threads in solid part files when we make the instruction of drawing the thread. To meet the document requirements of 3D printing (physical thread), a helix was first drawn and then scanned a triangle of the matched size along the helix to obtain the physical thread. The triangular thread guaranteed good sealing. After that, the original documents were converted to stereolithography (.STL) format for 3D printing. The file sketch (.STL format) used for printing is shown in Fig. 1a. Raised screw holes are used with the bolts containing inverted joints to seal the liquid.

ProJet 3500 HDMax (3D Systems, Inc., USA) was used to print these devices with reserved groove. The highest resolution of the printer is $750 \times 750 \times 1600$ DPI, which means that the minimum line width in xy plane is 34 μm and the minimum layer thickness is 16 μm . The depth of

Fig. 1 **a** Schematic of a 3D-printed file of STL format with virtual thread. Two threaded holes are inlet and outlet, respectively. The groove in the device is used to store and fix the magnets. **b** Device was obtained by ProJet 3500 HDMax after about 10 h of processing. **c** Dip the device (**b**) in plant oil and heat it in a water bath to clean the wax



the entire channel was 60 μm. This resolution is sufficient for the accuracy of 3D-printed microfluidic devices. The entire printing time lasts about 10 h. Two kinds of materials (photosensitive resin and wax) were used for printing the devices. The main part of the devices is a photosensitive resin that has good transparency after curing. Besides that, the filling and bottom of the devices are wax (milky substance in Fig. 1b). The wax was used as a filling and support material for the channel in printing process, and it was also a kind of sacrificed material for this device. The melting point of the wax is around 70 °C, which is far lower than the main part of the devices. Dipping the devices into plant oil, the wax can be easily removed by heating it in a water bath. In general, cleaning up the filling and support material (here means wax) in the device is critical for 3D printed microfluidics chips (Melchels et al. 2010; Zheng et al. 2012). After removing wax, the device is transparent and easy to observe (Fig. 1c). Therefore, this device is a good tool for particle manipulation.

2.2 Materials and experimental setup

Fluorescent polystyrene beads with a mean diameter of 5 μm (product no. G0500) and 12 μm (product no. 35-3) were purchased from Thermo Fisher Scientific. The particle solutions were prepared by mixing and re-suspending the fluorescent polystyrene beads in 0.5 × EMG 707 ferrofluid (Ferrotec Corp.) to a final concentration of 10⁶–10⁷ particles per milliliter. 0.5 vol% Tween 20 was added to the suspension to reduce particle aggregation and adhesions to the 3D-printed channel walls.

Two fingertight fittings were inserted into the devices (Fig. 2b). One was the inlet and the other was the outlet. This inverted cone connector fitting (Fig. 2a) has good airtightness and can effectively prevent liquid leakage. A high accurate syringe pump (LSP02-1B, LongerPump, Fig. 2c) connecting to the tube was used to pump the particle solution into the device. The groove in Fig. 2b was used to store and fix the permanent neodymium iron magnets (NdFeB, 5 × 5 × 5 mm³). The 3D-printed device was placed on the working stage of an inverted fluorescence microscope (DMi8, Leica). The excitation wavelength was 589 nm. The particle trajectories in the

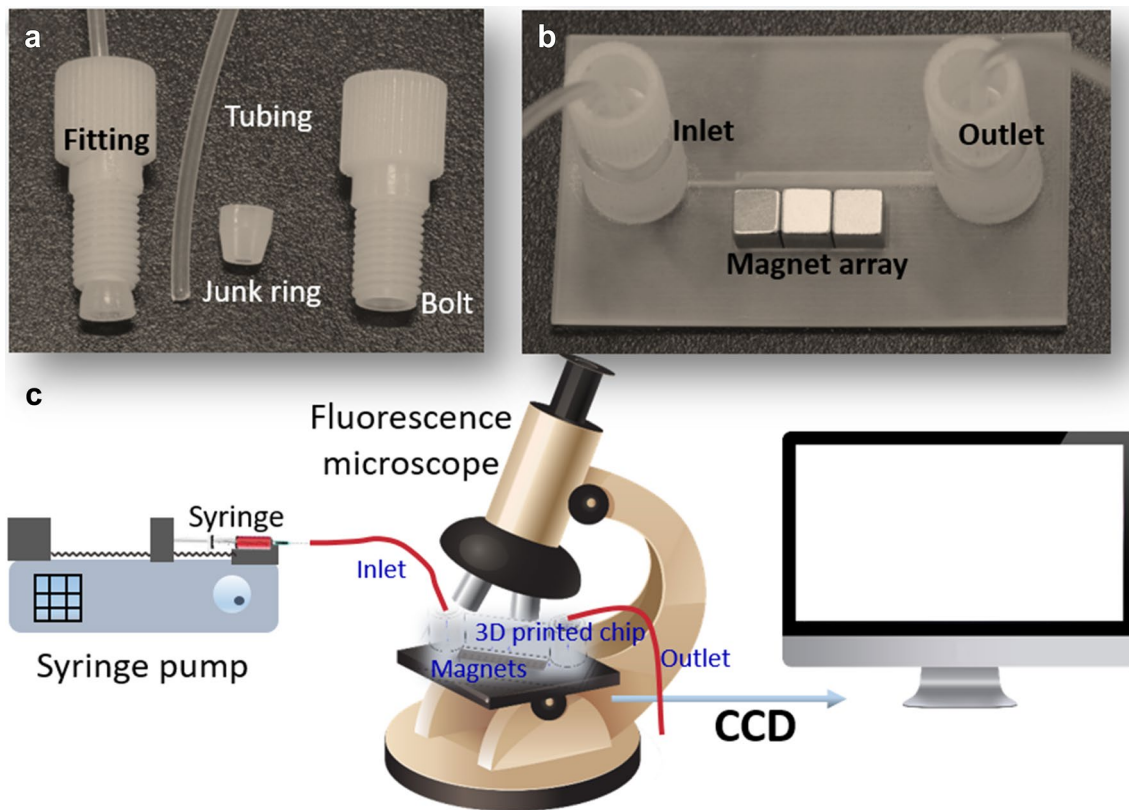


Fig. 2 a Commercial inverted cone connector fitting consists of an M1/4-28 bolt, a 1.6 mm ID junk ring, and a polyethylene tube (0.8 mm ID, 1.6 mm OD). b Photography of prototype device. Insert the fingertight fittings into the device with the integrated magnet

array. c Schematic of experimental setup. A high-precision syringe pump pushed ferrofluids mixed with dispersed diamagnetic particles into the 3D-printed device

manipulation device were visualized and recorded with a CCD camera (Nikon, Japan).

3 Theory and simulation

Figure 3a illustrates the channel and magnets dimension, as well as the position of magnets (distance of 5 mm to manipulation channel). The channel contains focused channel (10 mm×500 μm) and manipulation channel (25 mm×1500 μm). Diamagnetic particles were concentrated on the side close to the magnets by self-focusing channel. This effect can be achieved using a single magnet to focus the particles upstream. The magnet array consists of three 5 mm×5 mm×5 mm magnets.

To analyze the magnetic lateral deflection under different magnet arrays and flow rates, force balance should be considered to determine the trajectory of the particle in a magnetic field. In our study, diamagnetophoretic deflection of polystyrene micro-particles is dominated by magnetophoretic force and Stokes drag force (Hejazian and Nguyen 2015; Zhang et al. 2016). The negative magnetophoretic force acting on a point-like particle in magnetic induction B can be estimated as (Pamme 2006; Zhu et al. 2011)

$$F_m = 3 \frac{V_p}{\mu_0} \cdot \frac{\chi_p - \chi_f}{3 + \chi_p + \chi_f} (B \cdot \nabla) B, \tag{1}$$

where B is the magnetic flux density at center of the particle, and V_p is the volume of the particle. χ_p and χ_f are the magnetic susceptibility of the particle and ferrofluids, respectively. Permeability of vacuum $\mu_0 = 4\pi \times 10^{-7} \text{ N A}^{-2}$.

Because the magnetic susceptibility of polystyrene beads is lower than that of ferrofluids ($\chi_p < \chi_f$), the magnetophoretic force directs along the inverse direction of the magnetic field strength gradient. In addition, since both χ_p and χ_f are about three orders of magnitude smaller than 1, Eq. 1 can be written as (Hejazian et al. 2015)

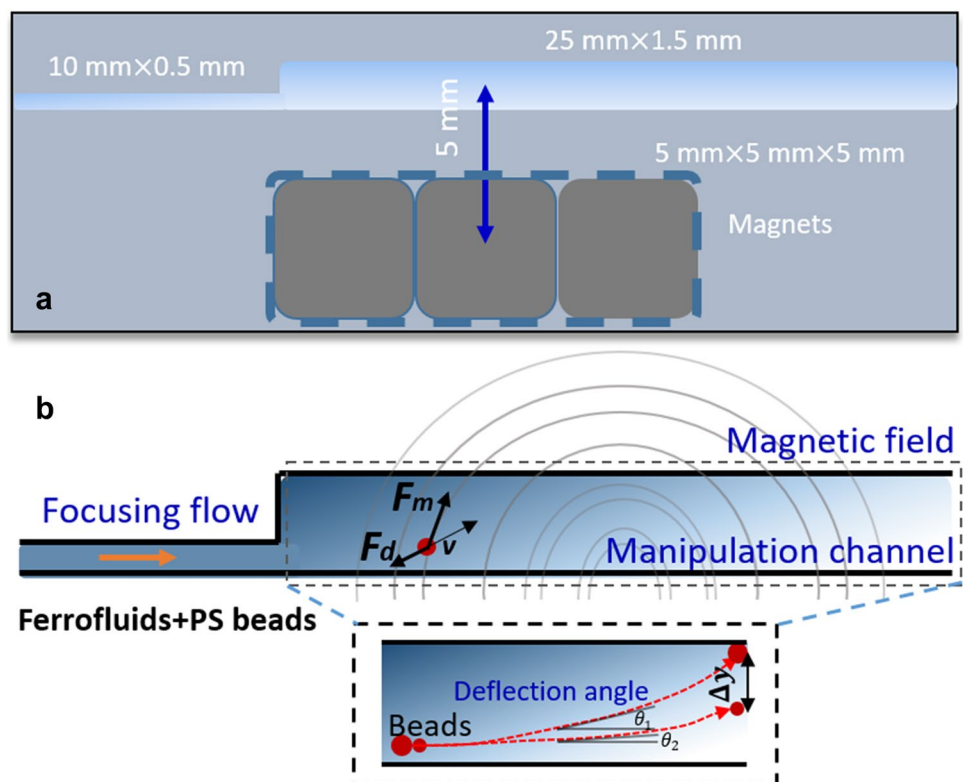
$$F_m = \frac{V_p}{\mu_0} (\chi_p - \chi_f) (B \cdot \nabla) B. \tag{2}$$

Hydrodynamic drag force arises when a particle moves in a different velocity with the surrounding fluid elements. The drag force on a moving spherical particle can be expressed as Eq. 3 (Iiguni et al. 2004):

$$F_d = 3\pi\eta D(\mathbf{v}_f - \mathbf{v}_p), \tag{3}$$

where η is viscosity of surrounding fluid, D is diameter of particle, and \mathbf{v}_f and \mathbf{v}_p are velocity vectors of surrounding fluid and the polystyrene beads dispersed in it. Figure 3b shows the force analysis of a particle in the channel. The direction of the hydrodynamic drag force was opposite to the direction of the velocity of the particle relative to the ferrofluids.

Fig. 3 **a** Detail view of the manipulation device. Self-focusing channel is 10 mm length and 500 μm width. The main manipulation channel contains 25 mm length and 1500 μm width. The center distance between the magnets and main manipulation channel is 5 mm. Three 5×5×5 mm³ magnets are used to separate particles from ferrofluids. The remnant field strength of each magnet is $B_r = 1.2 \text{ T}$. **b** Details of particles manipulation. The deflection angle of the particle trajectory is positively related to the particle size



Taking into account of these dominating and most effective particles forces, a numerical model for predicting of particle trajectories could be established by three parts of magnetic fields, single-phase laminar fluid flow through the microchannel, and particle tracing in COMSOL (COMSOL Lnc., USA).

In a current free region, the magnetic field is described using Maxwell–Ampere’s law, where

$$\nabla \times H = 0, \tag{4}$$

where H is the magnetic field strength. It is possible to define the scalar magnetic potential, V_m , from the relation:

$$H = -\nabla V_m. \tag{5}$$

Then, together with Gauss low for magnetic flux density, there is

$$\nabla \cdot (\mu_0 \mu_r H) = 0, \tag{6}$$

where μ_r is relative permeability. Magnetic insulation is considered around the whole system. In addition, a mathematical mode (“Coefficient Form PDE” in COMSOL) was used to calculate the magnetic flux density gradient.

In this low Reynolds number microfluidic flow, inertial part of the kinematic equation is negligible because of the tiny mass of polystyrene beads. No slip condition was applied along the walls of 3D-printed channel. The governing Navier–Stokes equation including the flow rate v is described as

$$\rho v \cdot \nabla v = f_b - \nabla p + \eta \nabla^2 v \tag{7}$$

and continuity equation:

$$\nabla \cdot (\rho \cdot v) = 0, \tag{8}$$

where p is the pressure, v is the fluid velocity, and ρ and η are the density and dynamic viscosity of fluid, respectively.

Finally, the balance equation can be simplified as

$$F_d + F_m = 0. \tag{9}$$

After substituting (9) into (2) and (3), the velocity can be inferred as

$$v_p = \frac{V_p (\chi_p - \chi_f) (B \cdot \nabla) B}{3\pi\eta D\mu_0}. \tag{10}$$

Treat the diamagnetic particle as a uniform sphere, then

$$V_p = \frac{\pi D^3}{6}. \tag{11}$$

Thus, Eq. (10) is simplified as

$$v_p = \frac{D^2 (\chi_p - \chi_f) (B \cdot \nabla) B}{6\eta\mu_0}. \tag{12}$$

The inset in Fig. 3b shows the trajectories of two particles. Larger particle corresponded to larger deflection angle. The

difference in deflection angles accounts for the particle sizes dependence in magnetic manipulation.

The parameter values used in the numerical simulations are listed in Table 1.

4 Results and discussion

4.1 Magnetic field

The Halbach array was proposed in 1980 (Halbach 1980). In our work, a groove was reserved in the printed microfluidic device. This kind of groove (Fig. 2b) could well constrain the magnets, so that they could be arranged in any type arrays. To characterize Halbach array, the magnetic field was simulated by COMSOL 4.4. We first calculated the magnetic flux density and its gradient. The magnetization of each magnet was set as 9.55×10^5 A/m according to the remnant field strength of $B_r = 1.2$ T. At the same time, we compared it with traditional alternating array. The magnetic field of alternating array was declining faster than that of Halbach array (Fig. 4a, b). It can be seen from the magnetic induction line that the magnetic field on one side is almost zero, while the other side can extend to a very distant position (Fig. 4a). Figure 4b shows that the magnetic fields on both sides of the alternating array were the same. Figure 4c, d describes the magnetic flux density inside the manipulation channel under the action of two type arrays in the form of contour lines. Figure 4e, f corresponds to the magnetic flux density gradient of the two arrays, respectively. In general, the magnetic flux density of Halbach array was larger than that of traditional alternating array at the same location. The difference was approximately from 30 to 70%. The gradient represented in Fig. 4e is slightly improved compared to alternating array (Fig. 4f).

Here, particle tracing for fluid flow was used to trace the particles’ trajectories with a time-dependent solver based on the results on magnetic fields and fluid flow. The force acted on the particles could be estimated as follows:

$$F_m = \mu_0 V_p (\chi_p - \chi_f) (B \cdot \nabla) B.$$

Table 1 Parameter values of numerical simulations

Parameter	Value
Relative permeability of magnet	1.05
Relative permeability of device and air	1
Relative permeability of PS beads	1
Relative permeability of ferrofluids	1.026
Fluid density (kg/m ³)	1000
Fluid dynamic viscosity (mPa s)	10
PS beads diameters (μm)	5 and 12
PS beads density (kg/m ³)	1050

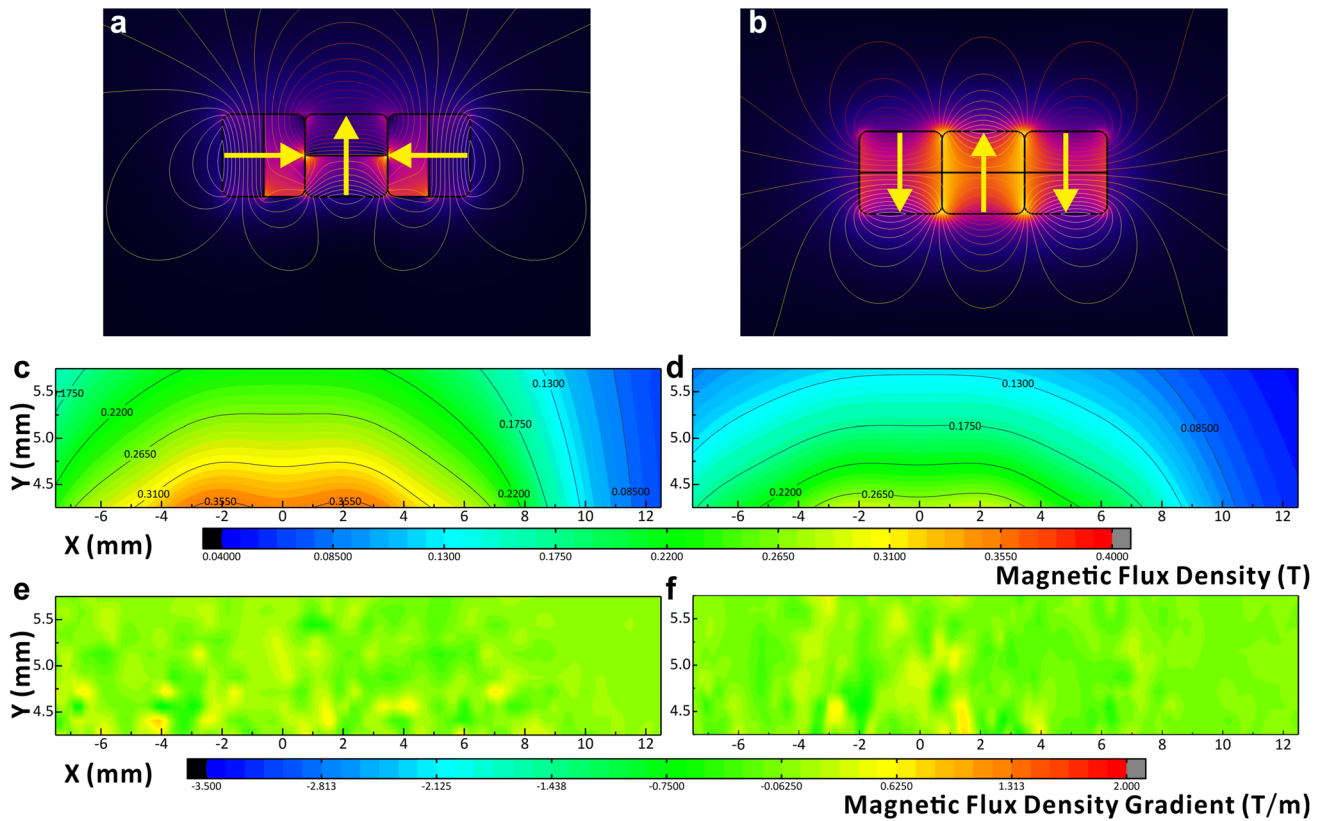


Fig. 4 Schematic design and magnetic simulations of Halbach array and traditional alternating array. Three cubic magnets construct these two kinds of arrays. The polarization angles of the magnets rotated 90° (a, Halbach array) or 180° (b, alternating array) in sequence. The yellow arrow indicates the direction of magnetic pole. Light yellow-

dashed lines represent the magnetic induction line. The magnetic field and its gradient distribution in the printed channel (c and e of Halbach array, d and f of alternating array). Magnetic flux density and its gradient at different locations were shown by contour lines with numerical values. (Color figure online)

This negative magnetophoretic force is proportional to magnetic flux density (B) and magnetic flux density gradient (∇B). We compared the B and ∇B values of Halbach and conventional alternating array configurations. Black lines in Fig. 5 shows that magnetic flux density generated by Halbach array was greater than that of alternating array. This was consistent with the situation in the printed channel (Fig. 4c, d). The magnetic flux density gradient of the two arrays was much more complicated. The values of the two arrays were not very different when they were close to the magnets' surface. Alternating array is sometimes larger (Fig. 5). However, with the increase of the distance from magnet (above 4 mm), the ∇B value of Halbach array was always larger than that of alternating array. Typically, in 3D-printed microfluidic device, the distance between the magnet and the manipulation channel is large. Therefore, alternating array can exert its manipulation efficiency well when it is applied to a minute manipulation device. Halbach array works well in this larger 3D-printed magnetic manipulation device for the long distance between sorting channel and magnets. The magnetometer measurement data

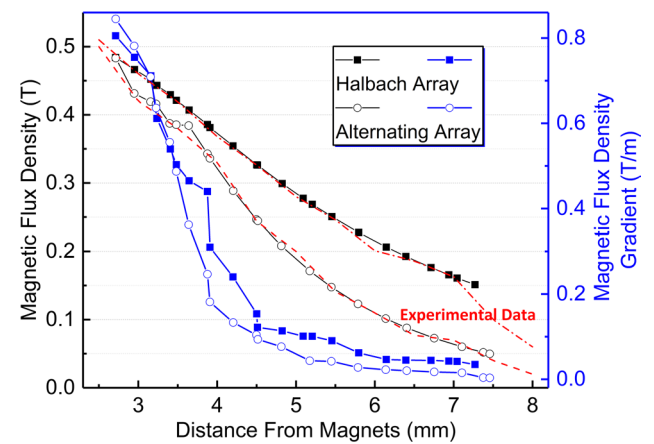


Fig. 5 Magnetic flux density (B , black lines) and its gradient (∇B , red lines) of two arrays plotted versus distance from magnets along central axis (the central axis was the middle yellow arrow in Fig. 4a, c.). The red-dotted lines were the curves of magnetic flux density (measured by a magnetometer) versus distance for both arrays. (Color figure online)

(red-dotted line in Fig. 5) are consistent with the numerical simulations' magnetic flux density data for both arrays. This verified the credibility of the numerical simulation.

4.2 Particle trajectories

Numerical simulations could point out the position of polystyrene beads with different sizes. Figure 6 shows the particle distribution in the magnified channel width direction of four different situations. The abscissa is -750 to 750 μm , corresponding to a 1500 μm -width 3D-printed channel. The cross section at inlet of channel is a 500 $\mu\text{m} \times 60$ μm rectangular. At low flow rate 1.08 mL/h , two sizes of particles could be well separated. About 80% 12 μm PS particles were pushed to the coordinates of 500 – 750 μm (yellow area) in the channel under the influence of Halbach array. The 5 μm PS particles were distributed over a wide channel width range (green area). When the flow rate was 1.08 mL/h , it can be inferred that particles of two

sizes could be well sorted via magnetic field generated by Halbach array (Fig. 6a). At the same flow rate, Fig. 6b shows the manipulation efficiency of two size particles decreased in alternating array. About 50% of the 12 μm particles' distribution overlaps with 5 μm particles. When the flow rate increased five times, the manipulation accuracy of two magnetic field arrays would be significantly worse (Fig. 6c, d). However, the particles' distribution coordinates of the Halbach array were still much better than alternating array.

Based on the results of the numerical simulations, it can be concluded that the magnetic field generated by Halbach array exhibited a better magnetic manipulation efficiency than the conventional alternating array. The magnetic field of such Halbach array has a clear advantage in the field of magnetic manipulation. More importantly, the large mutual forces that limit its application can be well constrained by the reserved grooves in the 3D-printed device. The experimental results show that this Halbach array-integrated device

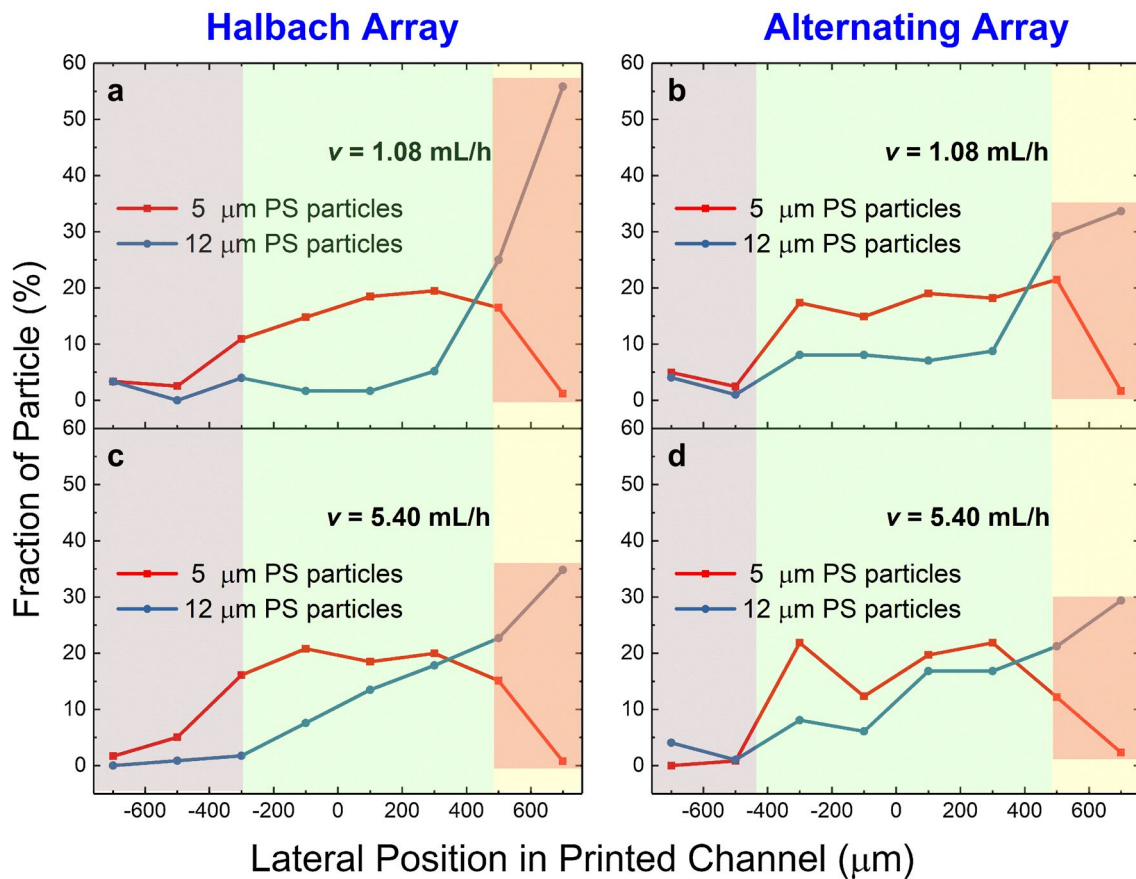


Fig. 6 Simulated distribution of different sizes polystyrene (PS) beads (red lines for 5 μm and blue lines for 12 μm in diameters). The width of the channel was divided into three areas (gray, green, and yellow). Gray area (-750 to -300 μm) had almost no particles. Green area (-300 to 500 μm) overlaps with two kinds of particle sizes. The yellow area (500 – 750 μm) was almost entirely 12 μm par-

ticles. The height of the red rectangle represented the percentage of separated particles. **a** Was the distribution of Halbach array and **b** was that of alternating array. The inlet volumetric flow rates were both 1.08 mL/h . **c**, **d** Also corresponded to these two arrays in sequence when the inlet volumetric flow rates were both 5.40 mL/h . (Color figure online)

can be used in the field of microfluidic magnetic manipulation and improve its efficiency.

To further confirm the negative magnetophoresis in ferrofluids, 5 μm red fluorescent polystyrene beads and 12 μm green fluorescent polystyrene beads were dispersed in $0.5 \times \text{EMG 707}$ ferrofluid to a final concentration of 10^6 – 10^7 particles per milliliter. Then, a high accurate syringe pump pumped the particle solution into a straight 500 μm -width microchannel. The magnetic array formed with 3 NdFeB magnets was placed on underside of the microchannel. The center distance between the magnet array and main manipulation channel was 5 mm. An inverted fluorescence microscope containing a CCD was used to observe the trajectory of the particles in the channel. The captured view field is approximately 500 $\mu\text{m} \times 400 \mu\text{m}$ rectangular.

Figure 7a, b shows the particle distribution for two magnet arrays. The two size particles dispersed in ferrofluids were sorted in different regions under the action of two magnet arrays. The 12 μm beads were distributed in the upper region, while most of the 5 μm beads were below them (Fig. 7a). This indicated excellent particles' size discrimination of the Halbach array. Under the same conditions, the distinction between the two beads in the width direction became less noticeable in alternating array in Fig. 7b. It can be concluded that the magnetic manipulation capability of Halbach array is better than that of traditional alternating array. These results are consistent with the conclusions of numerical simulations.

To characterize the particle manipulation capabilities of the magnet arrays, the two particles were also dispersed in ferrofluids, respectively. The concentration of the particles is similar to the mixed particle sample described above. By comparing the deflection angles, the particle trajectory under the action of the magnetic field could be visually displayed. Figure 8a, b shows the particles position without

and with fluorescence excitation. These two images showed that the particles were almost evenly distributed in the channel without magnetic array. When the magnetic field excitation was applied, the particle motion was deflected. Figure 8c–f shows the deflection angles of the particles in four different situations. Both magnetic arrays deflected the particle trajectory at the volumetric flow rate of 1.08 mL/h. However, the deflection angles of the particles by Halbach array (Fig. 8e) were greater than the deflection angle generated by traditional alternating array (Fig. 8c). On the other hand, the deflection angle of the particle trajectory decreased after increasing the volumetric flow rate. Corresponding to a volumetric flow rate of 5.40 mL/h, the deflection angles of alternating array (Fig. 6d) and Halbach array were 4.02° and 4.92° , respectively. These values were somewhat reduced compared to 5.54° (Fig. 8c, alternating array) and 7.29° (Fig. 8e, Halbach array) at a volumetric flow rate of 1.08 mL/h. Increasing the flow rate to five times makes the deflection effect of magnet array on the particles to be reduced. However, it can be stated that the effect of Halbach array is always better than that of alternating array.

Based on the above experimental results, we observed the trajectory of 12 μm polystyrene beads without or with Halbach array. Similar to the case of 5 μm particles, 12 μm particles were evenly distributed in the channel when no magnetic field was applied (Fig. 9a). The deflection angle of the particle trajectory was 17.97° (Fig. 9b), which was much larger than the 5 μm particle in the same situation (volumetric flow rate 1.05 mL/h, Halbach array). This shows that Halbach array in the 3D-printed device can well distinguish diamagnetic polystyrene beads of two particle sizes. The experimental phenomena here verify the reliability of the above numerical simulation results. To be able to separate more particles at the same time, we increase the volumetric flow rate. Here, the deflection angle of the

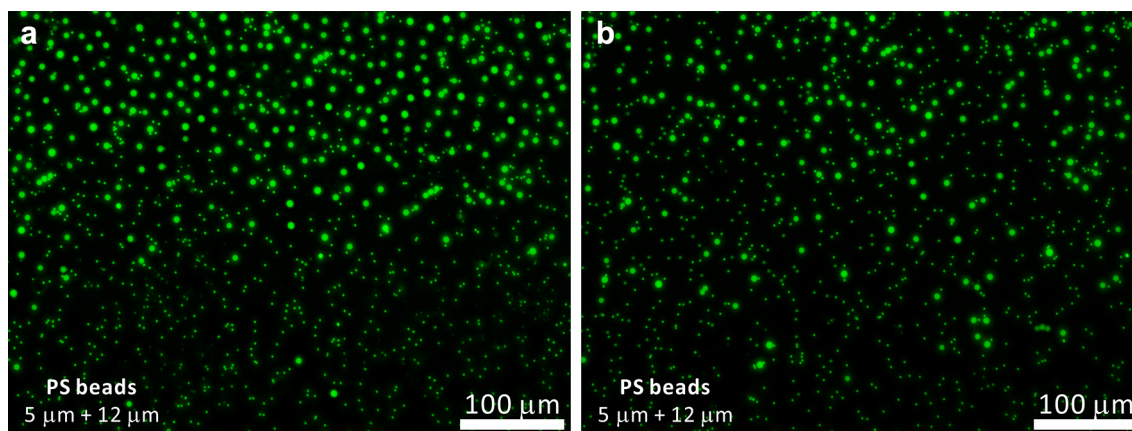


Fig. 7 Experimental results of diamagnetic 5 and 12 μm polystyrene beads in the 3D-printed channel under different magnetic field situations. The volumetric flow rate was 1.08 mL/h. The flow direction

was from left to right in all images. The distribution of polystyrene beads under **a** Halbach array, and **b** alternating array

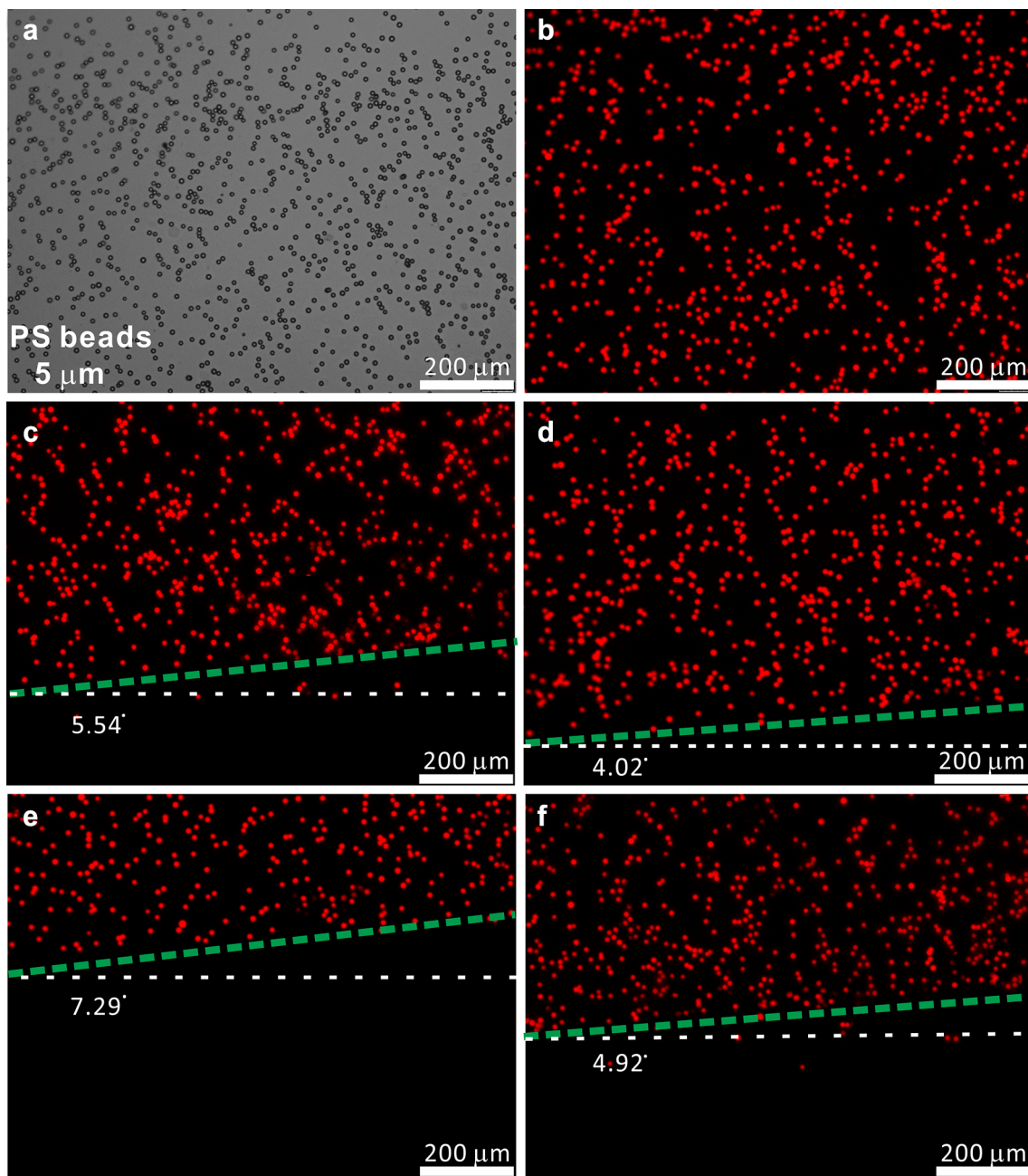


Fig. 8 **a** Distribution of polystyrene beads without magnetic field. **b–f** Fluorescence microscopy captures the particles distributions. **b** No magnetic field. The distribution of polystyrene beads under alternating array. The volumetric flow rate in **c** was 1.08 mL/h. The volumetric flow rate in **d** was 5.40 mL/h. The distribution of polystyrene beads under Halbach array. The volumetric flow rate in **e** was

1.08 mL/h. The volumetric flow rate in **f** was 5.40 mL/h. The green dashed lines were the boundaries of the particle trajectories (**c–f**). The angle (white text) between green-dotted line and horizontal white-dotted line is the deflection angle of the particle trajectory. (Color figure online)

particle trajectory has been reduced to a certain degree (14.81°, Fig. 9c), which will cause the overlapping of the position of two different particle sizes in the channel width direction. The numerical simulation results showed that when the flow rate was 5.40 mL/h, two different particle sizes could be distinguished by magnetic manipulation

(Halbach array). However, the difference in the width direction of the channel became worse. Increasing the flow rate can increase the efficiency of particle manipulation, but it will sacrifice the manipulation accuracy of particle size. In magnetic manipulation, the difference in particle size will decrease as the flow rate increase. Both

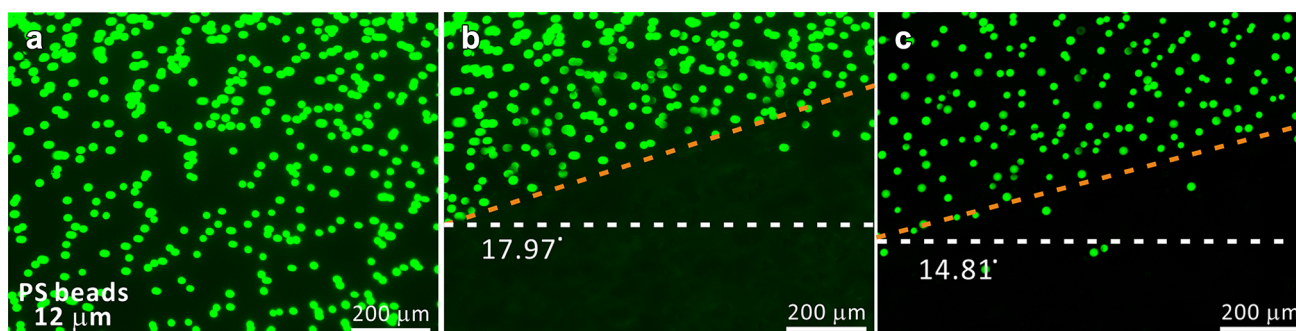


Fig. 9 **a** Distribution of polystyrene beads without magnetic field. **b** Distribution of polystyrene beads under Halbach array. The volumetric flow rate was 1.08 mL/h. **c** The distribution of polystyrene beads under Halbach array. The volumetric flow rate was 5.40 mL/h

numerical simulations and experimental results illustrate this conclusion.

5 Conclusion

This paper reported a 3D-printed microfluidic manipulation device with integrated magnet array. The trajectory of diamagnetic particles dispersed in diluted ferrofluids under two magnetic arrays was investigated. To cope with the relatively interaction forces between the magnets of Halbach array, we have reserved a groove to fix the magnets in the 3D-printed device. A high-precision 3D printer was chosen, and the photosensitive resin it used was easy to clean in this device. Meanwhile, the printed device has excellent transparency. 3D-printed channel was successfully applied to the research area of microfluidic magnetic separation for the first time. The effects of flow rate and magnetic field have been fully studied.

First, numerical calculation showed the magnetic field generated by the two arrays in the manipulation device. In particular, a detailed comparison about magnetic flux density and magnetic flux density gradients generated by Halbach array and conventional alternating array with respect to position was done. Moreover, the simulated magnetic flux density matched well to the magnetometer measurements. Due to the asymmetry of Halbach array, the magnetic flux and its gradient on magnets' one side were notably larger in the channel area of the device than that of the traditional alternating array. Thus, the array will be very suitable for magnetic manipulation.

Both numerical simulations and experiments were used to compare the efficiency of two arrays for magnetic manipulation. Numerical simulations show that the overlap of the two size particles in the channel width direction increases significantly as the flow rate increase (there is an increase in the proportion of particles that exist with the same coordinate.). However, Halbach array has much better particle manipulation

effect than that of alternating array at both low and high flow rate. Based on the numerical simulations, two size diamagnetic fluorescent particles (5 μm polystyrene beads and 12 μm polystyrene beads) were dispersed in ferrofluids for magnetic manipulation experiments, respectively. The deflection angle of large particle trajectories was significant larger than that of small particles under the same volumetric flow rate and magnetic field condition. Based on this, both arrays can achieve the purpose of magnetic separation for particle size in 3D-printed device. In addition, the experimental results also showed that the particle trajectory under the action of the Halbach array exhibited a larger deflection angle. Increasing the volumetric flow rate significantly reduced the time required for manipulation, but at the expense of the accuracy of magnetic sorting (the overlap of two particle sizes increases).

This work has pointed out that Halbach array can generate large magnetic flux density and magnetic flux density gradient, and it has obvious advantages in magnetic manipulation. In summary, due to the use of magnet arrays, the efficiency of magnetic manipulation is significantly increased. This paper used the 3D-printed device to easily constrain this Halbach array, making such an array very convenient for use in the field of microfluidic magnetic manipulation and increasing the efficiency of this significantly.

Acknowledgements Financial support from the National Natural Science Foundation of China (Grant No. 11572309 and 11572310), and the Strategic Priority Research Program of the Chinese Academy of Sciences (Grant No. XDB22040502) are gratefully acknowledged. This study was also supported by the Collaborative Innovation Center of Suzhou Nano Science and Technology. Thanks to the instrumentation support from engineering practice center of USTC. This work was partially carried out at the USTC Center for Micro and Nanoscale Research and Fabrication.

References

Au AK, Huynh W, Horowitz LF, Folch A (2016) 3D-printed microfluidics. *Angew Chem Int Ed* 55:3862–3881

- Cao QL, Liu MY, Wang Z, Han XT, Li L (2017) Dynamic motion analysis of magnetic particles in microfluidic systems under an external gradient magnetic field. *Microfluid Nanofluid* 21:11
- Cheng C, Wang S, Wu J, Yu Y, Li R, Eda S, Chen J, Feng G, Lawrie B, Hu A (2016) Bisphenol A sensors on polyimide fabricated by laser direct writing for onsite river water monitoring at attomolar concentration. *ACS Appl Mat Inter* 8:17784–17792
- Chudobova D, Cihalova K, Skalickova S, Zitka J, Rodrigo MAM, Milosavljevic V, Hynek D, Kopel P, Vesely R, Adam V (2015) 3D-printed chip for detection of methicillin-resistant *Staphylococcus aureus* labeled with gold nanoparticles. *Electrophoresis* 36:457–466
- Gervais T, El-Ali J, Gunther A, Jensen KF (2006) Flow-induced deformation of shallow microfluidic channels. *Lab Chip* 6:500–507
- Gholizadeh S, Shehata Draz M, Zarghooni M, Sanati-Nezhad A, Ghavami S, Shafiee H, Akbari M (2017) Microfluidic approaches for isolation, detection, and characterization of extracellular vesicles: current status and future directions. *Biosens Bioelectron* 91:588–605
- Gross BC, Erkal JL, Lockwood SY, Chen C, Spence DM (2014) Evaluation of 3D printing and its potential impact on biotechnology and the chemical sciences. *Anal Chem* 86:3240–3253
- Halbach K (1980) Design of permanent multipole magnets with oriented rare earth cobalt material. *Nucl Instrum Methods* 169:1–10
- Hejazian M, Nguyen NT (2015) Negative magnetophoresis in diluted ferrofluid flow. *Lab Chip* 15:2998–3005
- Hejazian M, Li W, Nguyen N-T (2015) Lab on a chip for continuous-flow magnetic cell separation. *Lab Chip* 15:959–970
- Ho CMB, Ng SH, Li KHH, Yoon Y-J (2015) 3D printed microfluidics for biological applications. *Lab Chip* 15:3627–3637
- Ibi T, Komada E, Furukawa T, Maruo S (2018) Multi-scale, multi-depth lithography using optical fibers for microfluidic applications. *Microfluid Nanofluid* 22:69
- Iguni Y, Suwa M, Watarai H (2004) High-magnetic-field electromagnetophoresis of micro-particles in a capillary flow system. *J Chromatogr A* 1032:165–171
- Johnston ID, McCluskey DK, Tan CKL, Tracey MC (2014) Mechanical characterization of bulk Sylgard 184 for microfluidics and microengineering. *J Micromech Microeng* 24:035017
- Kang JH, Driscoll H, Super M, Ingber DE (2016) Application of a Halbach magnetic array for long-range cell and particle separations in biological samples. *Appl Phys Lett* 108:5
- Khashan SA, Dagher S, Alazzam A (2018) Microfluidic multi-target sorting by magnetic repulsion. *Microfluid Nanofluid* 22:11
- Kim KS, Park JK (2005) Magnetic force-based multiplexed immunoassay using superparamagnetic nanoparticles in microfluidic channel. *Lab Chip* 5:657–664
- Kopp MRG, Arosio P (2018) Microfluidic approaches for the characterization of therapeutic proteins. *J Pharm Sci* 107:1228–1236
- Lee W, Kwon D, Chung B, Jung GY, Au A, Folch A, Jeon S (2014) Ultrarapid detection of pathogenic bacteria using a 3D immunomagnetic flow assay. *Anal Chem* 86:6683–6688
- Melchels FPW, Feijen J, Grijpma DW (2010) A review on stereolithography and its applications in biomedical engineering. *Biomaterials* 31:6121–6130
- Merola F, Memmolo P, Miccio L, Bianco V, Paturzo M, Ferraro P (2015) Diagnostic tools for lab-on-chip applications based on coherent imaging microscopy. *Proc IEEE* 103:192–204
- Minocchieri S, Burren JM, Bachmann MA, Stern G, Wildhaber J, Buob S, Schindel R, Kraemer R, Frey UP, Nelle M (2008) Development of the premature infant nose throat-model (PrINT-Model)—an upper airway replica of a premature neonate for the study of aerosol delivery. *Pediatr Res* 64:141
- Pamme N (2006) Magnetism and microfluidics. *Lab Chip* 6:24–38
- Qiu J, Liu X, Chen H, Xu X, Wen Y, Li P (2015) A low-frequency resonant electromagnetic vibration energy harvester employing the Halbach arrays for intelligent wireless sensor networks. *IEEE Trans Magn* 51:1–4
- Salauddin M, Halim M, Park J (2016) A magnetic-spring-based, low-frequency-vibration energy harvester comprising a dual Halbach array. *Smart Mater Struct* 25:095017
- Waheed S, Cabot JM, Macdonald NP, Lewis T, Guijt RM, Paull B, Bredmore MC (2016) 3D printed microfluidic devices: enablers and barriers. *Lab Chip* 16:1993–2013
- Walczak R, Adamski K (2015) Inkjet 3D printing of microfluidic structures—on the selection of the printer towards printing your own microfluidic chips. *J Micromech Microeng* 25:085013
- Wyatt Shields IVC, Reyes CD, Lopez GP (2015) Microfluidic cell sorting: a review of the advances in the separation of cells from debulking to rare cell isolation. *Lab Chip* 15:1230–1249
- Xia Y, Whitesides GM (1998) Soft lithography. *Annu Rev Mater Sci* 28:153–184
- Yan S, Zhang J, Yuan D, Zhao Q, Ma J, Li WH (2016) High-throughput, sheathless, magnetophoretic separation of magnetic and nonmagnetic particles with a groove-based channel. *Appl Phys Lett* 109:214101
- Yan S, Tan SH, Li Y, Tang S, Teo AJT, Zhang J, Zhao Q, Yuan D, Sluyter R, Nguyen NT, Li W (2017) A portable, hand-powered microfluidic device for sorting of biological particles. *Microfluid Nanofluid* 22
- Yazdi AA, Popma A, Wong W, Nguyen T, Pan Y, Xu J (2016) 3D printing: an emerging tool for novel microfluidics and lab-on-a-chip applications. *Microfluid Nanofluid* 20:1–18
- Zhang J, Yan S, Yuan D, Zhao Q, Tan SH, Nguyen NT, Li W (2016) A novel viscoelastic-based ferrofluid for continuous sheathless microfluidic separation of nonmagnetic microparticles. *Lab Chip* 16:3947–3956
- Zheng X, Deotte J, Alonso MP, Farquar GR, Weisgraber TH, Gemberling S, Lee H, Fang N, Spadaccini CM (2012) Design and optimization of a light-emitting diode projection micro-stereolithography three-dimensional manufacturing system. *Rev Sci Instrum* 83:125001
- Zhou Y, Xuan X (2016) Diamagnetic particle separation by shape in ferrofluids. *Appl Phys Lett* 109:102405
- Zhou J, Liang L, Xuan X (2016) Continuous-flow sheathless diamagnetic particle separation in ferrofluids. *J Magn Magn Mater* 412:114–122
- Zhou R, Bai F, Wang C (2017) Magnetic separation of microparticles by shape. *Lab Chip* 17:401–406
- Zhu J, Liang L, Xuan X (2011) On-chip manipulation of nonmagnetic particles in paramagnetic solutions using embedded permanent magnets. *Microfluid Nanofluid* 12:65–73